

Detrended fluctuation analysis of the magnetic and electric field variations that precede rupture

P. A. Varotsos,^{1,*} N. V. Sarlis,¹ and E. S. Skordas¹

¹*Solid State Section and Solid Earth Physics Institute, Physics Department, University of Athens, Panepistimiopolis, Zografos 157 84, Athens, Greece*

Magnetic field variations are detected before rupture in the form of ‘spikes’ of alternating sign. The distinction of these ‘spikes’ from random noise is of major practical importance, since it is easier to conduct magnetic field measurements than electric field ones. Applying detrended fluctuation analysis (DFA), these ‘spikes’ look to be random at short time-lags. On the other hand, long range correlations prevail at time-lags larger than the average time interval between consecutive ‘spikes’ with a scaling exponent α around 0.9. In addition, DFA is applied to recent preseismic electric field variations of long duration (several hours to a couple of days) and reveals a scale invariant feature with an exponent $\alpha \approx 1$ over all scales available (around five orders of magnitude).

Keywords: detrended fluctuation analysis, complex systems, scale invariance

PACS numbers:

Many physical and biological complex systems exhibit scale-invariant features characterized by long-range power-law correlations, which are often difficult to quantify due to the presence of erratic fluctuations, heterogeneity and nonstationarity embedded in the emitted signals. Here, we focus on different types of nonstationarities such as random spikes and pseudo-sinusoidal trends, that may affect the long-range correlation properties of signals that precede rupture. Since these nonstationarities may either be epiphenomena of external conditions or may arise from the intrinsic dynamics of the system, it is crucial to distinguish their origin. This is attempted in the present paper for both the magnetic and the electric field variations that appear before rupture by employing the detrended fluctuation analysis (DFA) as a scaling method to quantify long-range temporal correlations. In particular, for the magnetic field variations which have usually the form of ‘spikes’ of alternating sign, we find that at short time scales they look to be random (thus may then be confused with random noise), but at larger scales long-range correlations prevail. As for the electric field variations, that are usually superimposed on a pseudo-sinusoidal background, upon using the longest time series available to date (i.e., with duration up to a couple of days), a scale-invariant feature over five orders of magnitude emerges with an exponent close to unity.

I. INTRODUCTION

The detrended fluctuation analysis¹⁻⁹ (DFA) is a novel method that has been developed to address the problem of accurately quantifying long range correlations in non-stationary fluctuating signals. It has been already applied to a multitude of cases including DNA¹⁰⁻¹³, human motor activity¹⁴ and gait^{15,16}, car-

diac dynamics¹⁷⁻²⁰, meteorology^{21,22}, climate temperature fluctuations²³. Traditional methods such as power spectrum and autocorrelation analysis²⁴ are not suitable for non-stationary signals^{5,9}.

DFA is, in short, a modified root-mean-square (rms) analysis of a random walk and consists of the following steps: Starting with a signal $u(i)$, where $i = 1, 2, \dots, N$, and N is the length of the signal, the first step is to integrate $u(i)$ and obtain

$$y(i) = \sum_{j=1}^i [u(j) - \bar{u}] \quad (1)$$

where \bar{u} stands for the mean

$$\bar{u} = \frac{1}{N} \sum_{j=1}^N u(j). \quad (2)$$

We then divide the profile $y(i)$ into boxes of equal length n . In each box, we fit $y(i)$ using a polynomial function $y_n(i)$ which represents the local trend in that box. (If a different order l of polynomial fit is used, we have a different order DFA- l , for example DFA-1 if $l=1$, DFA-2 if $l=2$, etc.) Next, the profile $y(i)$ is detrended by subtracting the local trend $y_n(i)$ in each box of length n :

$$Y_n(i) = y(i) - y_n(i). \quad (3)$$

Finally, the rms fluctuation for the integrated and detrended signal is calculated

$$F(n) \equiv \sqrt{\frac{1}{N} \sum_{i=1}^N [Y_n(i)]^2}. \quad (4)$$

The behavior of $F(n)$ over a broad number of scales is obtained by repeating the aforementioned calculation of $F(n)$ for varied box length n . For scale invariant signals, we find:

$$F(n) \propto n^\alpha \quad (5)$$

where α is the scaling exponent. If $\alpha = 0.5$, the signal is uncorrelated (white noise), while if $\alpha > 0.5$ the signal is correlated.

By employing the DFA method it was found^{25,26} that long-range correlations exist in the original time-series of the so called seismic electric signals (SES) activities. These are low frequency ($\lesssim 1\text{Hz}$) electric signals preceding earthquakes²⁷⁻³², the generation of which could be understood in the following context. A change of pressure affects the thermodynamic parameters for the formation, migration or activation, in general, of defects in solids³³. In an ionic solid doped with aliovalent impurities a number of extrinsic defects is produced,^{34,35} due to charge compensation, a portion of which is attracted by nearby aliovalent impurities, thus forming electric dipoles that can change their orientation in space through a defect motion^{36,37}. Hence, pressure variations may affect the thermodynamic parameters of this motion, thus resulting in a decrease or increase³⁸ of the relaxation time of these dipoles, i.e., their (re)orientation is taking place faster or slower when an external electric field is applied. When the pressure, or the stress in general, reaches a *critical* value³⁹ a *cooperative* orientation of these electric dipoles occurs, which results in the emission of a transient electric signal. This may happen in the focal region of a (future) earthquake since it is generally accepted that the stress gradually changes there *before* rupture.

It has been shown^{40,41} that SES activities are better distinguished from electric signals emitted from man-made sources, if DFA is applied to a signal after it has been analyzed in a newly introduced time domain, termed natural time χ . In a time series comprising N events, the natural time $\chi_k = k/N$ serves as an index²⁵ for the occurrence of the k -th event. The evolution of the pair (χ_k, Q_k) is studied^{25,31,40-44}, where Q_k denotes a quantity proportional to the *energy* released in the k -th event. For dichotomous signals, which is frequently the case of SES activities, the quantity Q_k stands for the duration of the k -th pulse. The normalized power spectrum $\Pi(\omega) \equiv |\Phi(\omega)|^2$ was introduced, where

$$\Phi(\omega) = \sum_{k=1}^N p_k \exp\left(i\omega \frac{k}{N}\right) \quad (6)$$

and $p_k = Q_k / \sum_{n=1}^N Q_n$, $\omega = 2\pi\phi$; ϕ stands for the *natural frequency*. In natural time analysis, the properties of $\Pi(\omega)$ or $\Pi(\phi)$ are studied for natural frequencies ϕ less than 0.5, since in this range of ϕ , $\Pi(\omega)$ or $\Pi(\phi)$ reduces to a *characteristic function* for the probability distribution p_k in the context of probability theory. When the system enters the *critical* stage, the following relation holds^{25,31}:

$$\Pi(\omega) = \frac{18}{5\omega^2} - \frac{6 \cos \omega}{5\omega^2} - \frac{12 \sin \omega}{5\omega^3}. \quad (7)$$

For $\omega \rightarrow 0$, Eq.(7) leads to²⁵

$$\Pi(\omega) \approx 1 - 0.07\omega^2$$

which reflects³¹ that the variance of χ is given by

$$\kappa_1 = \langle \chi^2 \rangle - \langle \chi \rangle^2 = 0.07,$$

where $\langle f(\chi) \rangle = \sum_{k=1}^N p_k f(\chi_k)$. The entropy S in the natural time-domain is defined as⁴¹

$$S \equiv \langle \chi \ln \chi \rangle - \langle \chi \rangle \ln \langle \chi \rangle,$$

which depends on the sequential order of events⁴². It exhibits⁴³ concavity, positivity, Lesche^{45,46} stability, and for SES activities (critical dynamics) its value is smaller⁴¹ than the value $S_u (= \ln 2/2 - 1/4 \approx 0.0966)$ of a ‘‘uniform’’ (u) distribution (as defined in Refs.⁴⁰⁻⁴², e.g. when all p_k are equal or Q_k are positive independent and identically distributed random variables of finite variance. In this case, κ_1 and S are designated $\kappa_u (= 1/12)$ and S_u , respectively.). Thus, $S < S_u$. The same holds for the value of the entropy obtained^{43,44} upon considering the time reversal \mathcal{T} , i.e., $\mathcal{T}p_k = p_{N-k+1}$, which is labelled by S_- . In summary, the SES activities, in contrast to the signals produced by man-made electrical sources, when analyzed in natural time exhibit *infinitely* ranged temporal correlations^{40,41} and obey the conditions⁴⁴:

$$\kappa_1 = 0.07 \quad (8)$$

and

$$S, S_- < S_u. \quad (9)$$

For major earthquakes, i.e., with magnitude Mw6.5 or larger, SES activities are accompanied⁴⁷ by detectable variations of the magnetic field \mathbf{B} ⁴⁸. These variations, which are usually measured by coil magnetometers (see below), have the form of ‘spikes’ of alternating sign. It is therefore of interest to investigate whether these ‘spikes’ exhibit long range temporal correlations. This investigation, which is of major importance since only magnetic field data are usually available in most countries^{28,49,50} (since it is easier to conduct magnetic field measurements than electric field ones), is made here in Section II.

In the up to date applications of DFA, long-range correlations have been revealed in SES activities of duration up to a few hours^{25,26,40,41}. During the last few years, however, experimental results related to some SES activities of appreciably longer duration, i.e., from several hours to a couple of days, have been collected. These data now enable the investigation of scaling in a wider range of scales than hitherto known. This provides an additional scope of the present paper and is carried out in Section III. A discussion of the results concerning the magnetic and electric data follows in Section IV. Finally, our conclusions are presented in Section V.

II. MAGNETIC FIELD VARIATIONS PRECEDING RUPTURE

The measurements have been carried out by three DANSK coil magnetometers (DMM) oriented along the

three axes: EW, NS and vertical. Details on the calibration of these magnetometers can be found in the Supplementary Information of Ref.⁴⁷. In particular, this calibration showed that for periods larger than around half a second, the magnetometers measure⁵¹ the time derivative dB/dt of the magnetic field and their output is ‘neutralized’ approximately 200ms after the ‘arrival’ of a Heaviside unit step magnetic variation. It alternatively means that a signal recorded by these magnetometers should correspond to a magnetic variation that has ‘arrived’ at the sensor less than 200ms before the recording. The data were collected by a Campbell 21X datalogger with sampling frequency $f_{exp} = 1\text{sample/s}$.

Figure 1(a) provides an example of simultaneous recordings on April 18, 1995 at a station located close to Ioannina (IOA) city in northwestern Greece. Variations of both the electric (E) and magnetic field are shown. They were followed by a magnitude Mw6.6 earthquake (according to the Centroid Moment Tensor solutions reported by the United States Geological Survey) with an epicenter at $40.2^\circ\text{N}21.7^\circ\text{E}$ that occurred almost three weeks later, i.e., on May 13, 1995. The recordings of the two horizontal magnetometers oriented along the EW- and NS-directions labelled B_{EW} and B_{NS} , respectively, are shown in the lower two channels. They consist of a series of ‘spikes’ of alternating sign as it becomes evident in a 10min excerpt of these recordings depicted in Fig.1(b). These ‘spikes’ are superimposed on a background which exhibits almost pseudo-sinusoidal variations of duration much larger than 1s that are induced by frequent small variations of the Earth’s magnetic field termed magnetotelluric variations (MT). In addition, the horizontal E -variations were monitored at the same station by measuring the variation ΔV of the potential difference between (pairs of) electrodes - measuring dipoles- that are grounded at depths of $\approx 2\text{m}$. Several such dipoles were deployed along the EW- and NS-directions with lengths (L) a few to several tens of meters (short-dipoles) or a couple of km (long-dipoles) (Thus the electric field is given by $E = \Delta V/L$ and is usually measured in mV/km). For example, the following measuring dipoles are shown in the upper three channels of Fig.1(a): Two short electric dipoles at site ‘c’ of IOA station (see the Supplementary Information of Ref.⁴⁷ as well as Ref.⁵² where the selection of site ‘c’ has been discussed) of length 50m (labelled $E_c\text{-}W_c$ and $N_c\text{-}S_c$, respectively) while the uppermost channel corresponds to a long dipole (labelled $L'_s\text{-}I$) with length $\approx 5\text{km}$ at an almost NS-direction. As it becomes obvious in Fig.1(b), the E variations consist of a series of almost rectangular pulses (cf. the initiation and cessation of each rectangular pulse correspond to two ‘spikes’ with opposite sign in the B recordings).

We now apply DFA to the original time-series of the magnetic field variations and focus our attention on the B_{EW} component where the intensity of ‘spikes’ is higher. Dividing the time series of length N into N/n non-overlapping fragments, each of n observations, and deter-

mining the local trend of the sub-series we find the corresponding $\log F(n)$ versus $\log(n)$ plot where $n = f_{exp}\Delta t$ shown in Fig.2. If we fit the data with two straight lines (which are also depicted in Fig.2), the corresponding scaling exponents are $\alpha = 0.52 \pm 0.04$ and $\alpha = 0.89 \pm 0.03$ for the short- and long- time lags (i.e., smaller than around 12s and larger than $\approx 12\text{s}$), respectively. The crossover occurs at a value ($\Delta t \approx 12\text{s}$) which is roughly equal to the average duration $\langle T \rangle \approx 11.01 \pm 0.03\text{s}$ of each electric pulse, corresponding to the interval between two consecutive alternating ‘spikes’. Thus, Fig.2 shows that at time-lags Δt larger than $\langle T \rangle$ long-range power law correlations prevail (since $\alpha > 0.5$), while at shorter time-lags the α value is very close to that ($\alpha = 0.5$) of an uncorrelated signal (white noise).

The above findings are strikingly reminiscent of the case of signals with superposed *random* spikes studied by Chen et al.⁷. They reported that for a correlated signal with spikes, they found a crossover from uncorrelated behavior at small scales to correlated behavior at large scales with an exponent close to the exponent of the original stationary signal. They also investigated the characteristics of the scaling of the spikes only and found that the scaling behavior of the signal with *random* spikes is a superposition of the scaling of the signal and the scaling of the spikes. The case studied by Chen et al.⁷, however, is different from the present case, because the ‘spikes’ studied here correspond to the pre-seismic magnetic field variations and hence are *not* random (cf. recall that when applying DFA to the ‘durations’ of the electric field rectangular pulses shown in Fig.1(b), we found⁴⁰ an exponent around unity).

III. DFA OF SES ACTIVITIES OF LONG DURATION

In Fig.3 the following four long duration SES activities are depicted *all* of which have been recorded with sampling frequency $f_{exp} = 1\text{sample/s}$ at a station close to Pirgos (PIR) city located in western Greece (In this station only electric field variations are continuously monitored with a multitude of measuring dipoles the deployment of which has been described in detail in the Supplementary Information of Ref.⁵³). First, the SES activity on September 17, 2005 with duration of several hours that preceded the Mw6.7 earthquake with an epicenter at $36.3^\circ\text{N}23.3^\circ\text{E}$ on January 8, 2006. Second, the SES activity that lasted from January 21 until January 26, 2008 and preceded the Mw6.9 earthquake at $36.5^\circ\text{N}21.8^\circ\text{E}$ on February 14, 2008. Third, the SES activity during the period from February 29 to March 2, 2008 that was followed³² by a Mw6.4 earthquake at $38.0^\circ\text{N}21.5^\circ\text{E}$ on June 8, 2008 (SES activity information is issued *only* when the expected magnitude is around 6 units or larger^{44,53}). Finally, Fig.3(d) depicts the most recent SES activity of duration of several hours that was recorded on December 12, 2008. The latter SES activity

was followed by a Mw5.4 earthquake at 37.1°N20.8°E on February 16, 2009 (according to Athens Observatory the magnitude is $M_s(ATH)=M_L+0.5=6.0$; we clarify that predictions are issued *only* when the expected magnitude is comparable to 6.0 units or larger). Note that this earthquake occurred after the initial submission of the present paper (and its time of occurrence was approached⁵⁴ by means of the procedure developed in Ref.³²).

Here, we analyze, as an example, the long duration SES activity that lasted from February 29 until March 2, 2008(Fig.3(c)). The time-series of this electrical disturbance, which is not of obvious dichotomous nature, is depicted in the upper channel (labelled “a”) of Fig.4. The signal, comprising a number of pulses, is superimposed on a background which exhibits frequent small MT variations. The latter are simultaneously recorded at *all* measuring sites, in contrast to the SES activities that solely appear at a restricted number of sites depending on the epicentral region of the future earthquake³⁹. This difference provides a key for their distinction. In order to separate the background, we proceed into the following steps: First, we make use of another measuring dipole of the same station, i.e., the channel labelled “b” in Fig.4, which has not recorded the signal but does show the MT pseudo-sinusoidal variations. Second, since the sampling rate of the measurements is 1sample/s, we now compute the increments every 1s of the two time-series of channels “a” and “b”. Assuming the “1s increments” of channel “a” lying along the x-axis and those of “b” along the y-axis, we plot in the middle panel of Fig.4 (labeled “c”) the angle of the resulting vector with dots. When a non-MT variation (e.g., a dichotomous pulse) appears (disappears) in channel “a”, this angle in “c” abruptly changes to 0° ($\pm 180^\circ$). Thus, the dots in panel “c” mark such changes. In other words, an increased density of dots (dark regions) around 0° or $\pm 180^\circ$ marks the occurrence of these pulses, on which we should focus. To this end, we plot in channel “d” of Fig.4 the residual of a linear least squares fit of channel “a” with respect to channel “b”. Comparing channel “d” with channel “a”, we notice a significant reduction of the MT background but not of the signal. The small variations of the MT background that still remain in “d”, are now marked by the light blue line, which when removed result in channel “e” of Fig.4. Hence, channel “e” solely contains the electric field variations that precede rupture. This channel provides the time-series which should now be analyzed.

The DFA analysis (in conventional time) of the time-series of channel “e” of Fig.4 is shown in Fig.5. It reveals an almost linear $\log F(n)$ vs $\log n$ plot (where $n = f_{exp}\Delta t$) with an exponent $\alpha \approx 1$ practically *over all scales available* (approximately five orders of magnitude). Note, that this value of the exponent remains the same irrespective if we apply DFA-1, DFA-2 or DFA-3. This result is in agreement with the results obtained^{25,26,40,41} for SES activities of *shorter* duration.

For the classification of this signal, i.e., to distinguish

whether it is a true SES activity or a man-made electric signal, we now proceed to its analysis in natural time. In order to define (χ_k, Q_k) the individual pulses of the signal depicted in channel “e” of Fig.4 have to be identified. A pulse starts, of course, when the amplitude exceeds a given threshold and ends when the amplitude falls below it. Moreover, since the signal is not obviously dichotomous, instead of finding the duration of each pulse, one should sum the “instantaneous power” during the pulse duration in order to find Q_k , as already mentioned. To this end, we plot in Fig.6 the histogram of the instantaneous power P of channel “e” of Fig.4, computed by squaring its amplitude. An inspection of this figure reveals a bimodal feature which signifies the periods of inactivity ($P < 500\mu V^2Hz$) and activity ($P > 500\mu V^2Hz$) in channel “e” of Fig.4. In order to find Q_k , we focus on the periods of activity and select the power threshold P_{thres} around the second peak of the histogram in Fig.6. Let us consider, for example, the case of $P_{thres}=1400\mu V^2Hz$. In Fig.7(a), we depict the instantaneous power P of the signal in channel “e” of Fig.4. Starting from the beginning of the signal, we compare P with P_{thres} and when P exceeds P_{thres} we start summing up the P values until P falls below P_{thres} for the first time, $k = 1$. The resulting sum corresponds to Q_1 . This procedure is repeated until P falls below P_{thres} for the second time, $k = 2$, and the new sum represents Q_2 , etc. This leads to the natural time representation depicted in Fig.7(b). The result depends, of course, on the proper selection of P_{thres} . The latter can be verified by checking whether a small change of P_{thres} around the second peak of the histogram, leads to a natural time representation resulting in approximately the same values of the parameters κ_1 , S and S_- . By randomly selecting P_{thres} in the range 500 to 2000 μV^2Hz , we obtain that the number of pulses in channel “e” of Fig.4 is $N = 1100 \pm 500$ with $\kappa_1 = 0.070 \pm 0.007$, $S = 0.082 \pm 0.012$ and $S_- = 0.078 \pm 0.006$. When P_{thres} ranges between 1000 to 1500 μV^2Hz , the corresponding values are $N = 1200 \pm 200$ with $\kappa_1 = 0.068 \pm 0.003$, $S = 0.080 \pm 0.005$ and $S_- = 0.074 \pm 0.003$. Thus, we observe that irrespective of the P_{thres} value chosen, the parameters κ_1 , S and S_- obey the conditions (8) and (9) for the classification of this signal as SES activity. The same holds for a non-dichotomous signal recorded on March 28, 2009 at Keratea station located close to Athens (Fig.8). To approach the occurrence time of the impending event, the procedure developed in Ref.³² has been employed for the seismicity within the area $N_{37.7}^{38.8}E_{22.6}^{24.1}$. The results, when considering the seismicity until early in the morning on June 19, 2009, are shown in Fig.9. They show that a local maximum of the probability³² $Prob(\kappa_1)$ of the seismicity is observed at $\kappa_1 = 0.070$ upon the occurrence of the following events: (a) an $M_L=3.2$ event at 12:42 UT on June 18 with epicenter at 38.7N 23.0E and an $M_L=3.2$ event at 03:44 UT on June 19 at 37.9N 23.0E if we take a magnitude threshold $M_{thres}=3.0$ (b) when taking $M_{thres}=3.1$, the maximum occurs again upon the occurrence of the aforementioned event at 12:42 on June

18 (c) when increasing the threshold at $M_{thres}=3.2$, the maximum occurs somewhat earlier, i.e., upon the occurrence of the $M_L=3.5$ event at 08:26 UT on June 18 at 38.7N 23.0E. Let us now consider a larger area, i.e., $N_{37.65}^{39.00}E_{22.20}^{24.10}$, and repeat the same calculation. The results are shown in Fig.10. They reveal again the occurrence of a local maximum of $\text{Prob}(\kappa_1)$ at $\kappa_1 = 0.070$ upon the occurrence of the above mentioned $M_L=3.2$ event at 12:42 UT on June 18 when considering either $M_{thres}=3.2$ (Fig.10(c)) or $M_{thres}=3.1$ (Fig.10(b)) (for the latter case a maximum also occurs at the last event shown in the figure with $M_L=3.2$ at 03:44 UT on June 19). The maximum appears upon the occurrence of a $M_L=3.0$ at 23:48 UT on June 18 when decreasing the threshold at $M_{thres}=3.0$.

In summary, the results exhibit both magnitude- and spatial- invariance, which is characteristic when approaching the critical point.

Note added on July 21, 2009. Repeating the aforementioned calculation for the area $N_{37.65}^{39.00}E_{22.20}^{24.10}$, we find the results depicted in Fig.11(a) for $M_{thres}=2.8$. An inspection of this figure reveals a local maximum of $\text{Prob}(\kappa_1)$ at $\kappa_1 = 0.070$ upon the occurrence of a $M_L=3.0$ at 21:10 UT on July 19, 2009 with an epicenter at 38.1N 22.7E (the same result is found for $M_{thres}=2.9$.) Interestingly, this local maximum turns to be the prominent one when studying the seismicity in the same area (for the same threshold $M_{thres}=2.8$) since June 21, 2009, see Fig.11(b); the same holds for $M_{thres}=3.0$. Furthermore, the latter study was made for the smaller area $N_{37.7}^{38.8}E_{22.6}^{24.1}$ for $M_{thres}=2.6, 2.7$ and 3.0 and showed a local maximum of $\text{Prob}(\kappa_1)$ at $\kappa_1 = 0.070$ upon the occurrence of the same event (i.e., at 21:10 UT on July 19, 2009). The investigation still continues in order to clarify whether the latter local maximum will eventually turn to become a prominent one.

Note added on September 5, 2009. At 8:17 UT on September 2, 2009, a $M_L=4.3$ earthquake occurred almost at the center of the predicted area $N_{37.7}^{38.8}E_{22.6}^{24.1}$. The continuation of the investigation of the previous paragraph in the smaller area $N_{37.8}^{38.8}E_{22.6}^{24.1}$ showed a prominent maximum of $\text{Prob}(\kappa_1)$ at $\kappa_1 = 0.070$ (see Fig.12 (a)) upon the occurrence of a $M_L=3.3$ event at 09:35 UT on September 2, 2009, with an epicenter at 38.1N 23.3E. This was found to hold for the aforementioned larger area (see Fig.12 (b)) as well, thus revealing that the *criticality* condition -as developed in Ref. 32- is obeyed.

Note added on September 19, 2009. The previous Note was followed by three earthquakes of magnitude 4.4, 4.7 and 4.8 that occurred at 21:15 UT September 9, 06:04 UT September 10 and 07:12 UT September 16, 2009 with epicenters at 38.7N 22.8E, 38.3N 24.1E and 39.0N 22.2E, respectively. The continuation of the natural time investigation of the seismicity for $M_{thres}=3.0$ in the smaller area $N_{37.7}^{38.8}E_{22.6}^{24.1}$ revealed a prominent maximum $\text{Prob}(\kappa_1)$ at $\kappa_1 = 0.070$ (see Fig.13 (a)) upon the occurrence of a $M_L=3.0$ event at 01:55 UT on September 18, 2009, with epicenter at 38.7N22.8E. Since the same was found to be

true for the aforementioned larger area as well (see Fig.13 (b)), the investigation is now extended to additional magnitude thresholds in order to clarify whether (beyond spatial and) magnitude threshold invariance holds, thus identifying that the system approaches the *critical* point.

Note added on October 13, 2009. The previous note was actually followed by an earthquake of magnitude 4.6 that occurred at 22:27 UT on October 2, 2009 with an epicenter at 38.3N 22.9E. The natural time investigation of the seismicity still continues with the following results. First, in the smaller area $N_{37.7}^{38.8}E_{22.6}^{24.1}$: For $M_{thres}=2.7$, the criticality condition started to be approached since October 7 and the *most prominent* maximum of $\text{Prob}(\kappa_1)$ at $\kappa_1 = 0.070$ was observed upon the occurrence of the $M_L=2.7$ event at 01:56 UT on October 11, 2009. The same behavior was found for $M_{thres}=2.8$ (but the last event for this case occurred at 08:15UT on October 10, 2009 at 38.2N 23.1E). Second, in the larger area $N_{37.65}^{39.00}E_{22.20}^{24.10}$: For both thresholds $M_{thres}=2.7$ and $M_{thres}=2.8$, the criticality condition was also started to be approached since 20:18 UT on October 7, 2009. The *most prominent* maximum of $\text{Prob}(\kappa_1)$ at $\kappa_1 = 0.070$ for $M_{thres}=2.7$ have been observed upon the occurrence of the aforementioned $M_L=2.7$ event at 01:56 UT on October 11, 2009, while for $M_{thres}=2.8$ it was observed at 4:51 UT on October 9, 2009, upon the occurrence of the $M_L=2.9$ event at 38.1E 23.2E. Interestingly, the results for the larger area are almost identical if the investigation starts at 15:00 UT on July 31, 2009.

Note added on November 14, 2009. Meanwhile, two SES activities were recorded at PAT on October 24 and November 11, 2009, see Fig.14. Hence, the *ongoing* study (Fig.15) of the previous Note should be accompanied by a complementary study, focused on the determination of the occurrence time of the impending mainshock, that also considers the seismicity in the western part (i.e., $N_{37.5}^{38.6}E_{19.8}^{22.2}$) of the PAT selectivity map (see area A in Fig.8 of Ref.³²). Such a complementary study, when taking into account the seismic data until early in the morning on November 13, 2009, leads to the results depicted in Fig.16 for $M_{thres}=3.1$. A local maximum of $\text{Prob}(\kappa_1)$ at $\kappa_1 = 0.070$ was observed (see the rightmost arrow in Fig.16) upon the occurrence of $M_L=3.2$ event at 18:55 UT on November 2, 2009 (that was followed by a $M_L=5.6$ EQ at 05:25 UT on November 3, 2009, with an epicenter at 37.4°N 20.4°E). In addition, the *most prominent* maximum in Fig.16 of $\text{Prob}(\kappa_1)$ at $\kappa_1 = 0.070$ is observed later, i.e., upon the occurrence of a $M_L=3.1$ event at 01:42 UT on November 13, 2009 (see the leftmost arrow in Fig.16). This, which has been also checked for $M_{thres}=3.0$, provides evidence that the critical point is approached. Calculations are now carried out to further investigate the magnitude threshold invariance of this behavior.

Note added on November 27, 2009. Actually, after the previous Note the following two earthquakes occurred at 18:30 UT on November 16, 2009 and at 04:29 UT on November 19, 2009 with magnitudes ($M_s(\text{ATH})$) 4.3 and

4.4 and epicenters at $38.4^\circ\text{N } 22.0^\circ\text{E}$ and $38.2^\circ\text{N } 22.7^\circ\text{E}$, respectively, that both lie within the PAT selectivity map, i.e. $\text{N}_{37.5}^{38.6}\text{E}_{19.8}^{23.3}$. The continuation of the two studies mentioned in the previous Note, i.e., in the PAT selectivity map as well as in the area $\text{N}_{37.65}^{39.09}\text{E}_{22.2}^{24.1}$, both show that the *most prominent* maximum of $\text{Prob}(\kappa_1)$ at $\kappa_1 = 0.070$ was observed upon the occurrence of the $M_L=3.2$ event at 19:31 UT on November 25, 2009, thus indicating that the system is near the critical point.

Note added on February 9, 2010. Two earthquakes with magnitudes $M_s(\text{ATH})(= M_L + 0.5)=5.7$ and 5.6 occurred at $38.4^\circ\text{N } 22.0^\circ\text{E}$ (and hence inside the expected area) at 15:56 UT on January 18 and at 00:46 UT on January 22, 2010 (after observing a maximum of $\text{Prob}(\kappa_1)$ versus κ_1 at $\kappa_1=0.070$ for $M_{\text{thres}}=3.1$ upon the occurrence of the $M_L=3.2$ event at 15:56 UT on January 15, 2010). These two magnitudes are consistent with the condition $M_s(\text{ATH})\geq 6.0$ (under which SES information are publicized) if a reasonable⁵⁵ experimental error $3\sigma=0.7$ is accepted.

However, since the amplitudes of all the SES activities recorded could warrant an impending mainshock with magnitude exceeding $M_s(\text{ATH})=6.0$, and in order to determine the occurrence time of such a mainshock, if any, the natural time analysis of seismicity still continues. This analysis starting at 04:00 UT on December 27, 2009, revealed that in the area $\text{N}_{38.0}^{39.0}\text{E}_{21.5}^{23.7}$ (almost $200\text{km} \times 100\text{km}$) the criticality condition (i.e., $\text{Prob}(\kappa_1)$ versus κ_1 maximizes at $\kappa_1=0.070$) for $M_{\text{thres}}=3.5$ is obeyed during the last three events of Fig.17, the latest of which (that exhibits the strongest maximum) occurred at 10:18 UT on February 7, 2010 at $38.6^\circ\text{N } 23.7^\circ\text{E}$ with $M_L=4.3$. This has been checked to be valid for broader areas as well (spatial invariance), but has not yet been found to be confirmed (until early in the morning on February 8, 2010) for lower magnitude thresholds. The investigation of the latter is still in progress, because the following might happen: Due to coarse-graining the criticality condition might have been obeyed at a larger time-window for large magnitude thresholds, while for smaller thresholds the time-window may become smaller thus achieving a better accuracy in the determination of the occurrence time of the impending earthquake.

IV. DISCUSSION

In general, electric field variations are interconnected with the magnetic field ones through Maxwell equations. Thus, it is intuitively expected that when the former exhibit long range correlations the same should hold for the latter. This expectation is consistent with the present findings which show that, at long time-lags, the original time-series of both electric- and magnetic field variations

preceding rupture exhibit DFA-exponents close to unity.

The above can be verified when data of both electric- and magnetic-field variations are simultaneously available. This was the case of the data presented in Fig.1. In several occasions, however, as mentioned in Section I, only magnetic field data exist, in view of the fact that it is easier to conduct magnetic field measurements compared to the electric field ones. When using coil magnetometers, the magnetic field variations have the form of series of ‘spikes’. Whenever the amplitude of these ‘spikes’ significantly exceed the pseudo-sinusoidal variations of the MT background, as in the case of B_{EW} in Fig.1, a direct application of DFA (see Fig.2) elucidates the long range correlations in the magnetic field variations preceding rupture. On the other hand, when considerable pseudo-sinusoidal MT variations are superimposed, a direct application of DFA is not advisable. One must first subtract the MT variations (following a procedure similar to that used in the electric field data in Fig.4) and then apply DFA.

The preceding paragraph refers to the analysis of the signal in conventional time. As already shown in Ref.⁴¹, natural time analysis, has the privilege that allows the distinction between true SES activities and man made signals. This type of analysis, however, demands the knowledge of the energy released during each consecutive event. The determination of this energy is easier to conduct in the case of electric field variations (this is so, because coil magnetometers, as mentioned in Section II, act as dB/dt detectors). When these variations are of clear dichotomous nature, the energy release is proportional to the duration of each pulse^{40,41}. On the other hand, in absence of an obvious dichotomous nature an analysis of the ‘instantaneous power’ similar to that presented in the last paragraph of Section III should be carried out to determine the parameters κ_1 , S and S_- in natural time.

V. CONCLUSIONS

First, DFA was used as a scaling analysis method to investigate long-range correlations in the original time series of the magnetic field variations that precede rupture and have the form of ‘spikes’ of alternating sign. We find a scaling exponent α close to 0.9 for time-lags larger than the average time interval $\langle T \rangle$ between consecutive ‘spikes’, while at shorter time-lags the exponent is close to 0.5 thus corresponding to uncorrelated behavior.

Second, using electric field data of long duration SES activities (i.e., from several hours to a couple of days) recorded during the last few years, DFA reveals a scale invariant feature with an exponent $\alpha \approx 1$, over *all* scales available (approximately five orders of magnitude).

* Electronic address: pvaro@otenet.gr

¹ C.-K. Peng, J. Mietus, J. M. Hausdorff, S. Havlin, H. E.

- Stanley, and A. L. Goldberger, *Phys. Rev. Lett.* **70**, 1343 (1993).
- ² C.-K. Peng, S. V. Buldyrev, S. Havlin, M. Simons, H. E. Stanley, and A. L. Goldberger, *Phys. Rev. E* **49**, 1685 (1994).
 - ³ S. V. Buldyrev, A. L. Goldberger, S. Havlin, R. N. Mantegna, M. E. Matsa, C.-K. Peng, M. Simons, and H. E. Stanley, *Phys. Rev. E* **51**, 5084 (1995).
 - ⁴ M. S. Taqqu, V. Teverovsky, and W. Willinger, *Fractals* **3**, 785 (1995).
 - ⁵ P. Talkner and R. O. Weber, *Phys. Rev. E* **62**, 150 (2000).
 - ⁶ K. Hu, P. C. Ivanov, Z. Chen, P. Carpena, and H. E. Stanley, *Phys. Rev. E* **64**, 011114 (2001).
 - ⁷ Z. Chen, P. C. Ivanov, K. Hu, and H. E. Stanley, *Phys. Rev. E* **65**, 041107 (2002).
 - ⁸ Z. Chen, K. Hu, P. Carpena, P. Bernaola-Galvan, H. E. Stanley, and P. C. Ivanov, *Phys. Rev. E* **71**, 011104 (2005).
 - ⁹ L. Xu, P. C. Ivanov, K. Hu, Z. Chen, A. Carbone, and H. E. Stanley, *Phys. Rev. E* **71**, 051101 (2005).
 - ¹⁰ S. M. Ossadnik, S. B. Buldyrev, A. L. Goldberger, S. Havlin, R. N. Mantegna, C. K. Peng, M. Simons, and H. E. Stanley, *Biophys. J.* **67**, 64 (1994).
 - ¹¹ R. N. Mantegna, S. V. Buldyrev, A. L. Goldberger, S. Havlin, C. K. Peng, M. Simons, and H. E. Stanley, *Phys. Rev. Lett.* **73**, 3169 (1994).
 - ¹² R. N. Mantegna, S. V. Buldyrev, A. L. Goldberger, S. Havlin, C. K. Peng, M. Simons, and H. E. Stanley, *Phys. Rev. Lett.* **76**, 1979 (1996).
 - ¹³ P. Carpena, P. Bernaola-Galván, P. C. Ivanov, and H. E. Stanley, *Nature (London)* **418**, 955 (2002).
 - ¹⁴ K. Hu, P. C. Ivanov, Z. Chen, M. F. Hilton, H. E. Stanley, and S. A. Shea, *Physica A* **337**, 307 (2004).
 - ¹⁵ J. M. Hausdorff, Y. Ashkenazy, C. K. Peng, P. C. Ivanov, H. E. Stanley, and A. L. Goldberger, *Physica A* **302**, 138 (2001).
 - ¹⁶ Y. Ashkenazy, J. M. Hausdorff, P. C. Ivanov, and H. E. Stanley, *Physica A* **316**, 662 (2002).
 - ¹⁷ P. C. Ivanov, A. Bunde, L. A. Nunes Amaral, S. Havlin, J. Fritsch-Yelle, R. M. Baevsky, H. E. Stanley, and A. L. Goldberger, *Europhys. Lett.* **48**, 594 (1999).
 - ¹⁸ S. Havlin, S. V. Buldyrev, A. Bunde, A. L. Goldberger, P. C. Ivanov, C. K. Peng, and H. E. Stanley, *Physica A* **273**, 46 (1999).
 - ¹⁹ H. E. Stanley, L. A. Nunes Amaral, A. L. Goldberger, S. Havlin, P. C. Ivanov, and C. K. Peng, *Physica A* **270**, 309 (1999).
 - ²⁰ P. C. Ivanov, L. A. Nunes Amaral, A. L. Goldberger, and H. E. Stanley, *Europhys. Lett.* **43**, 363 (1998).
 - ²¹ K. Ivanova and M. Ausloos, *Physica A* **274**, 349 (1999).
 - ²² K. Ivanova, T. P. Ackerman, E. E. Clothiaux, P. C. Ivanov, H. E. Stanley, and M. Ausloos, *J. Geophys. Res.-Atmospheres* **108 D9**, 4268 (2003).
 - ²³ E. Koscielny-Bunde, A. Bunde, S. Havlin, H. E. Roman, Y. Goldreich, and H. J. Schellnhuber, *Phys. Rev. Lett.* **81**, 729 (1998).
 - ²⁴ R. L. Stratonovich, *Topics in the theory of random noise Vol. I* (Gordon and Breach, New York, 1981).
 - ²⁵ P. A. Varotsos, N. V. Sarlis, and E. S. Skordas, *Phys. Rev. E* **66**, 011902 (2002).
 - ²⁶ A. Weron, K. Burnecki, S. Mercik, and K. Weron, *Phys. Rev. E* **71**, 016113 (2005).
 - ²⁷ P. Varotsos and K. Alexopoulos, *Tectonophysics* **110**, 73 (1984).
 - ²⁸ A. C. Fraser-Smith, A. Bernardi, P. R. McGill, M. E. Ladd, R. A. Helliwell, and O. G. Villard, *Geophys. Res. Lett.* **17**, 1465 (1990).
 - ²⁹ S. Uyeda, T. Nagao, Y. Orihara, T. Yamaguchi, and I. Takahashi, *Proc. Natl. Acad. Sci. USA* **97**, 4561 (2000).
 - ³⁰ S. Uyeda, M. Hayakawa, T. Nagao, O. Molchanov, K. Hattori, Y. Orihara, K. Gotoh, Y. Akinaga, and H. Tanaka, *Proc. Natl. Acad. Sci. USA* **99**, 7352 (2002).
 - ³¹ P. A. Varotsos, N. V. Sarlis, H. K. Tanaka, and E. S. Skordas, *Phys. Rev. E* **72**, 041103 (2005).
 - ³² N. V. Sarlis, E. S. Skordas, M. S. Lazaridou, and P. A. Varotsos, *Proc. Japan Acad., Ser. B* **84**, 331 (2008).
 - ³³ P. Varotsos, K. Alexopoulos, and K. Nomicos, *Phys. Status Solidi B* **111**, 581 (1982).
 - ³⁴ D. Kostopoulos, P. Varotsos, and S. Mourikis, *Can. J. Phys.* **53**, 1318 (1975).
 - ³⁵ P. Varotsos, *J. Phys. Chem. Sol.* **42**, 405 (1981).
 - ³⁶ P. Varotsos and K. Alexopoulos, *J. Phys. Chem. Sol.* **41**, 443 (1980).
 - ³⁷ P. Varotsos and K. Alexopoulos, *Phys. Status Solidi B* **42**, 409 (1981).
 - ³⁸ P. Varotsos and K. Alexopoulos, *Phys. Rev. B* **21**, 4898 (1980).
 - ³⁹ P. Varotsos and K. Alexopoulos, *Thermodynamics of Point Defects and their Relation with Bulk Properties* (North Holland, Amsterdam, 1986).
 - ⁴⁰ P. A. Varotsos, N. V. Sarlis, and E. S. Skordas, *Phys. Rev. E* **67**, 021109 (2003).
 - ⁴¹ P. A. Varotsos, N. V. Sarlis, and E. S. Skordas, *Phys. Rev. E* **68**, 031106 (2003).
 - ⁴² P. A. Varotsos, N. V. Sarlis, E. S. Skordas, and M. S. Lazaridou, *Phys. Rev. E* **70**, 011106 (2004).
 - ⁴³ P. A. Varotsos, N. V. Sarlis, H. K. Tanaka, and E. S. Skordas, *Phys. Rev. E* **71**, 032102 (2005).
 - ⁴⁴ P. A. Varotsos, N. V. Sarlis, E. S. Skordas, H. K. Tanaka, and M. S. Lazaridou, *Phys. Rev. E* **73**, 031114 (2006).
 - ⁴⁵ B. Lesche, *J. Stat. Phys.* **27**, 419 (1982).
 - ⁴⁶ B. Lesche, *Phys. Rev. E* **70**, 017102 (2004).
 - ⁴⁷ P. A. Varotsos, N. V. Sarlis, and E. S. Skordas, *Phys. Rev. Lett.* **91**, 148501 (2003).
 - ⁴⁸ N. Sarlis and P. Varotsos, *J. Geodyn.* **33**, 463 (2002).
 - ⁴⁹ D. Karakelian, G. C. Beroza, S. L. Klemperer, and A. C. Fraser-Smith, *Bull. Seism. Soc. Am.* **92**, 1513 (2002).
 - ⁵⁰ O. A. Molchanov, Y. A. Kopytenko, P. M. Voronov, E. A. Kopytenko, T. G. Matiashvili, A. C. Fraser-Smith, and A. Bernardi, *Geophys. Res. Lett.* **19**, 1495 (1992).
 - ⁵¹ P. Varotsos, N. Sarlis, and E. Skordas, *Proc. Jpn. Acad., Ser. B: Phys. Biol. Sci.* **77**, 87 (2001).
 - ⁵² P. A. Varotsos, N. V. Sarlis, and E. S. Skordas, *Appl. Phys. Lett.* **86**, 194101 (2005).
 - ⁵³ P. A. Varotsos, N. V. Sarlis, E. S. Skordas, H. K. Tanaka, and M. S. Lazaridou, *Phys. Rev. E* **74**, 021123 (2006).
 - ⁵⁴ P. A. Varotsos, N. V. Sarlis, E. S. Skordas, and M. S. Lazaridou (2009), cond-mat/0707.3074v3.
 - ⁵⁵ P. Varotsos, *The Physics of Seismic Electric Signals* (TerraPub, Tokyo, 2005).

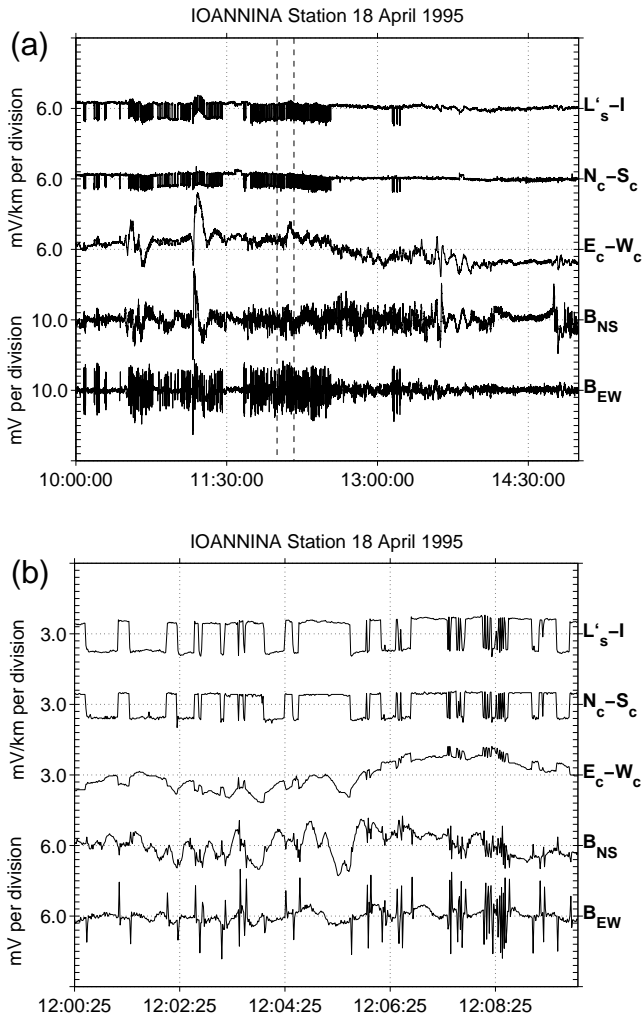


FIG. 1: (a):Variations of the electric- (upper three channels) and magnetic- (lower two channels) field recorded on April 18, 1995 (see the text). (b):A 10min excerpt of (a). The two dashed lines in (a) show the excerpt depicted in (b).

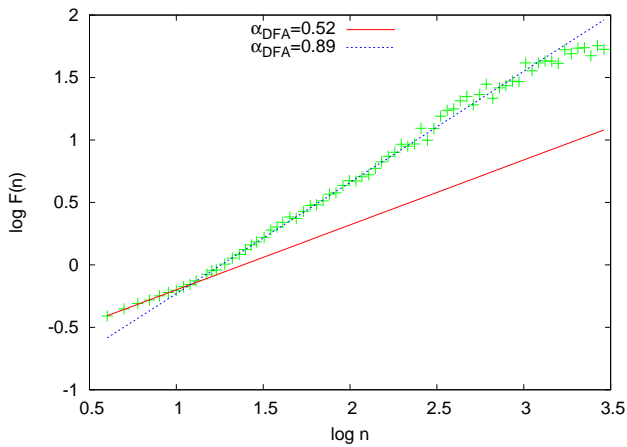


FIG. 2: (color online)The DFA for the B_{EW} channel of Fig.1(a). Logarithm base 10 is used.

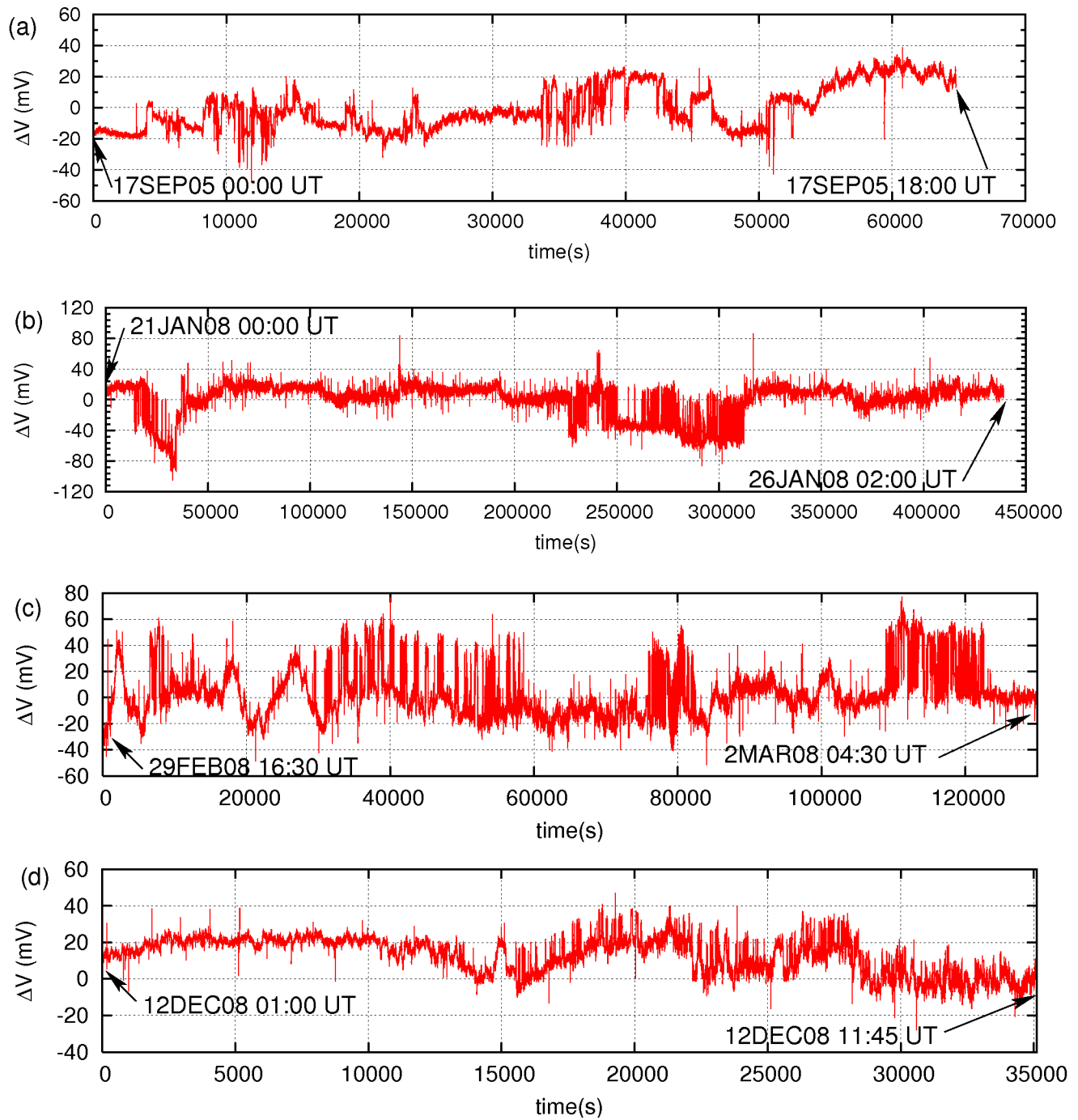


FIG. 3: (color online) Long duration SES activities during the last few years (see the text).

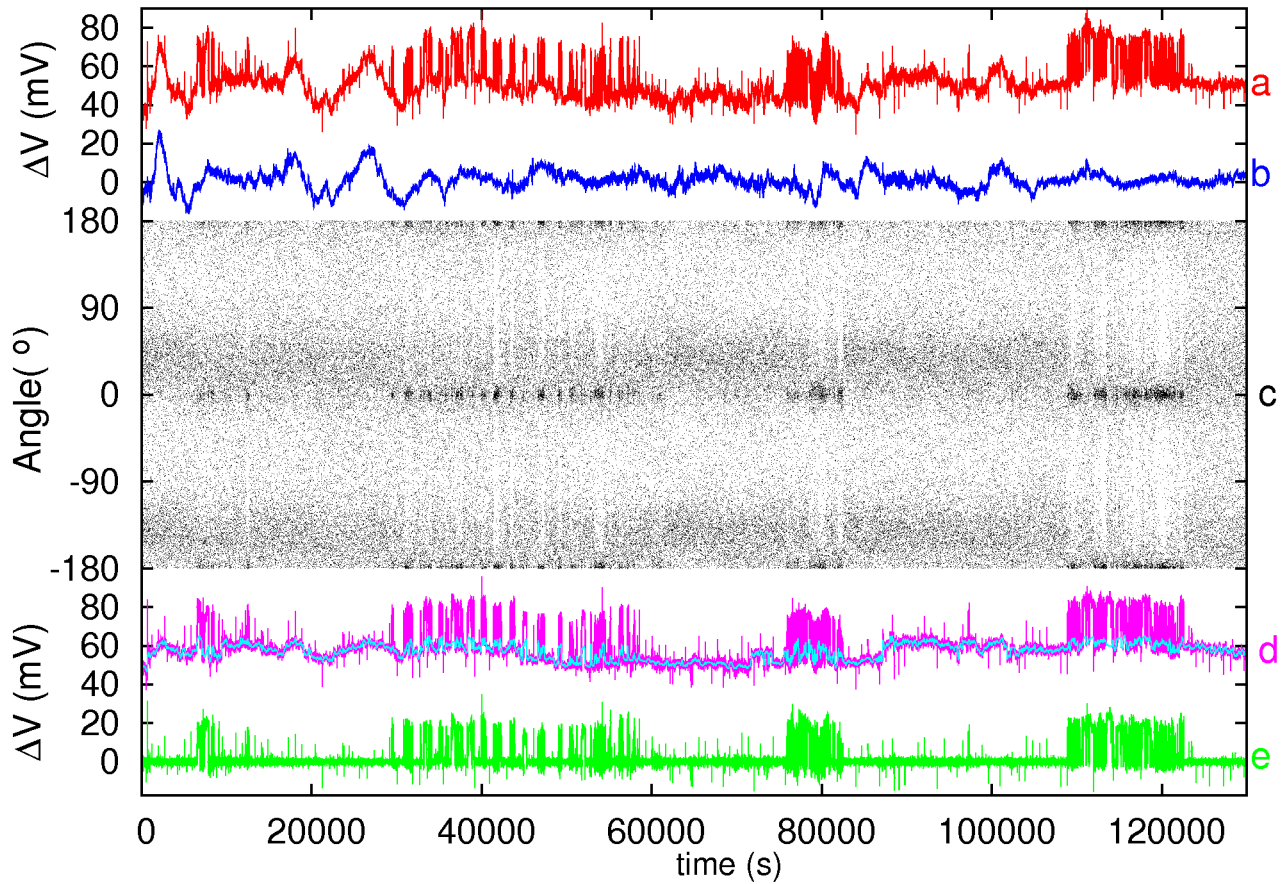


FIG. 4: (color online) The long duration SES activity from February 29 to March 2, 2008. Channel “a”:original time series, channel “b”: recordings at a measuring dipole which did not record the SES activity, but does show MT variations, “c”:the angle of the resulting vector upon assuming that the “1s increments” of channel “a” lie along the x-axis and those of channel “b” along the y-axis. Channel “d”: the residual of a linear least squares fit of channel “a” with respect to channel “b”, channel “e”:the same as “d” but after eliminating the slight variations of the background. For the sake of clarity, channels “a”, “b” and “d” have been shifted vertically.

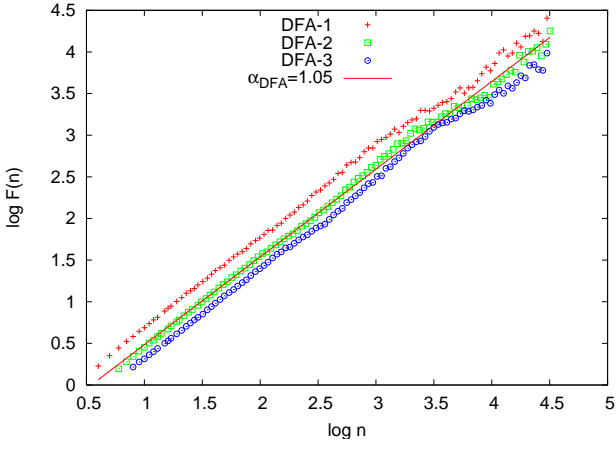


FIG. 5: (color online) The DFA- l ($l=1,2$ and 3) for the lower channel (i.e., the one labelled “e”) of Fig.4. Logarithm base 10 is used.

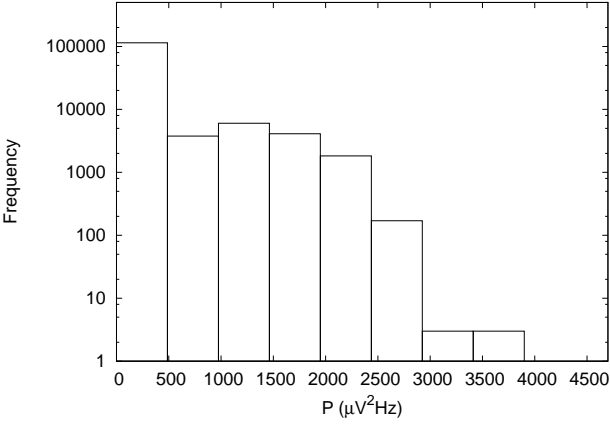


FIG. 6: Histogram of the “instantaneous power” P , i.e., the squared amplitude of the signal depicted in channel “e” of Fig.4.

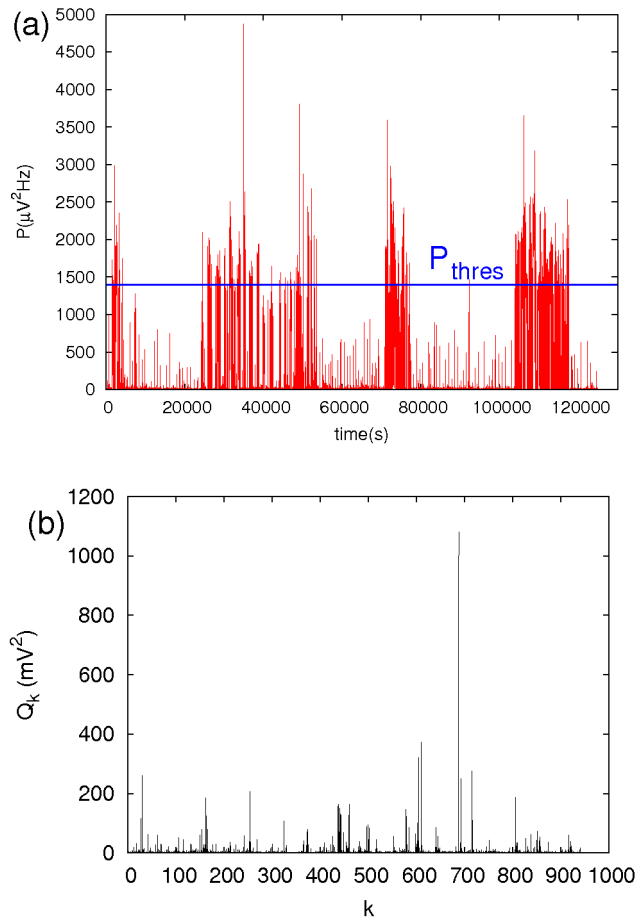


FIG. 7: (color online) (a) The “instantaneous power” P of the signal depicted in channel “e” of Fig.4 (computed by squaring its amplitude). The solid line parallel to the x-axis marks an example of a threshold $P_{\text{thres}} (=1400 \mu\text{V}^2\text{Hz})$ chosen. (b) The resulting representation of the signal depicted in channel “e” of Fig.4 in natural time, when considering $P_{\text{thres}}=1400 \mu\text{V}^2\text{Hz}$.

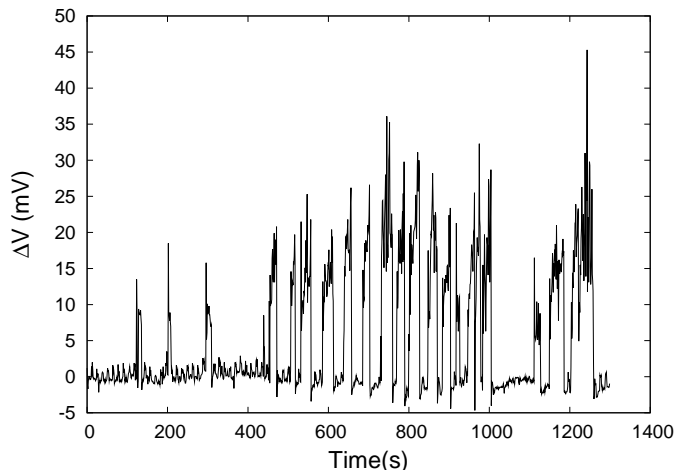


FIG. 8: The most recent electric signal analyzed (see the text).

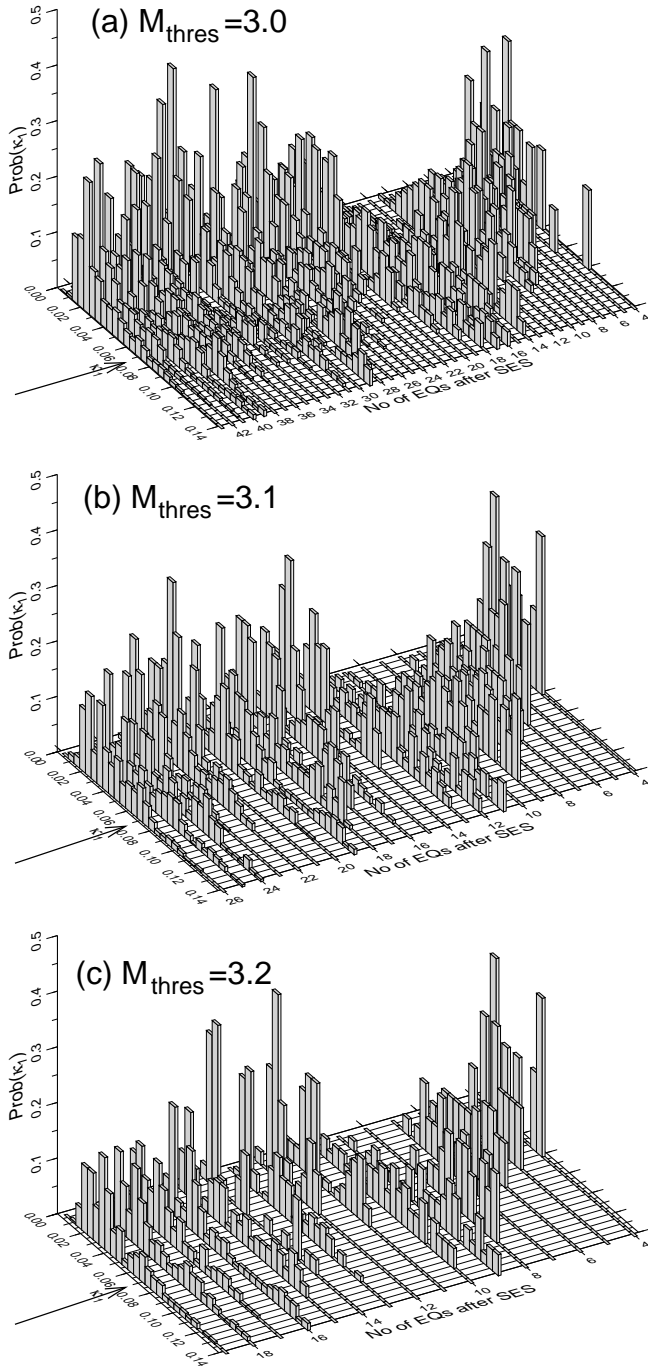


FIG. 9: The probability $Prob(\kappa_1)$ of the seismicity within the area $N_{37.7}^{38.8} E_{22.6}^{24.1}$ subsequent to the SES activity recorded at KER on March 28, 2009, when considering the following magnitude thresholds: $M_{thres}=3.0$ (a), 3.1 (b) and 3.2 (c).

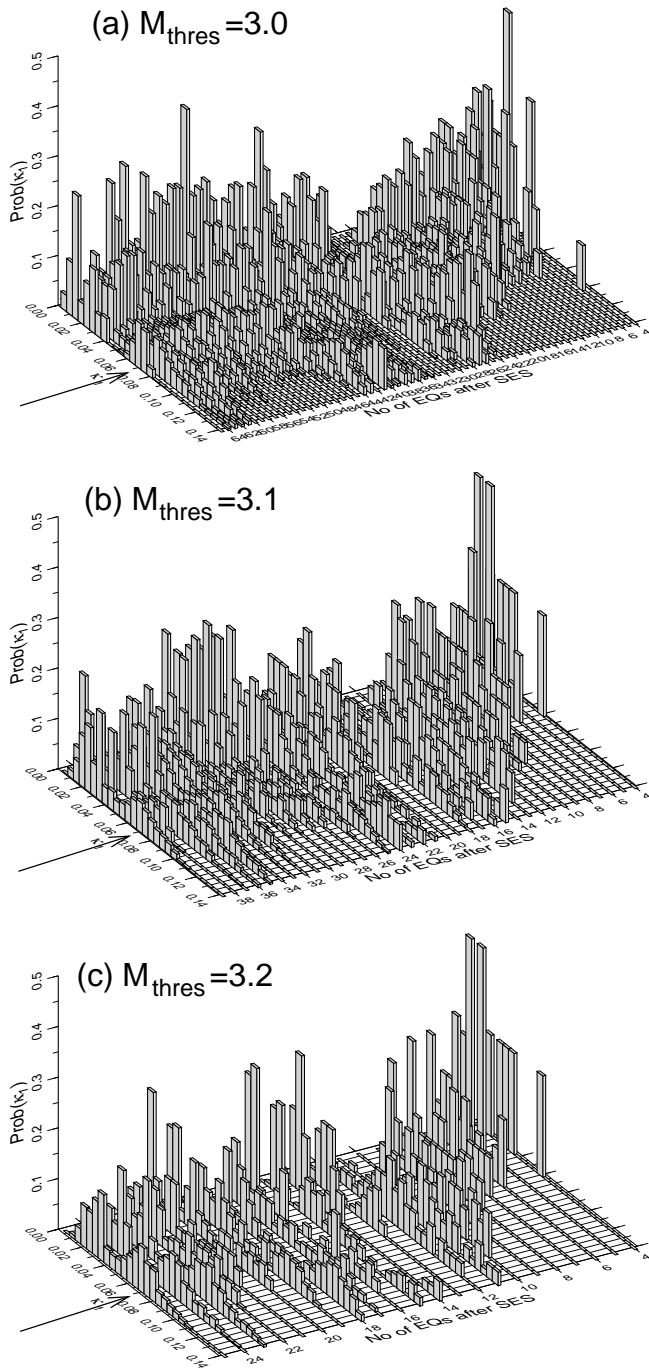


FIG. 10: The same as Fig.9, but for the area $N_{37.65}^{39.00}E_{22.20}^{24.10}$ in order to check the spatial invariance of the results (see the text).

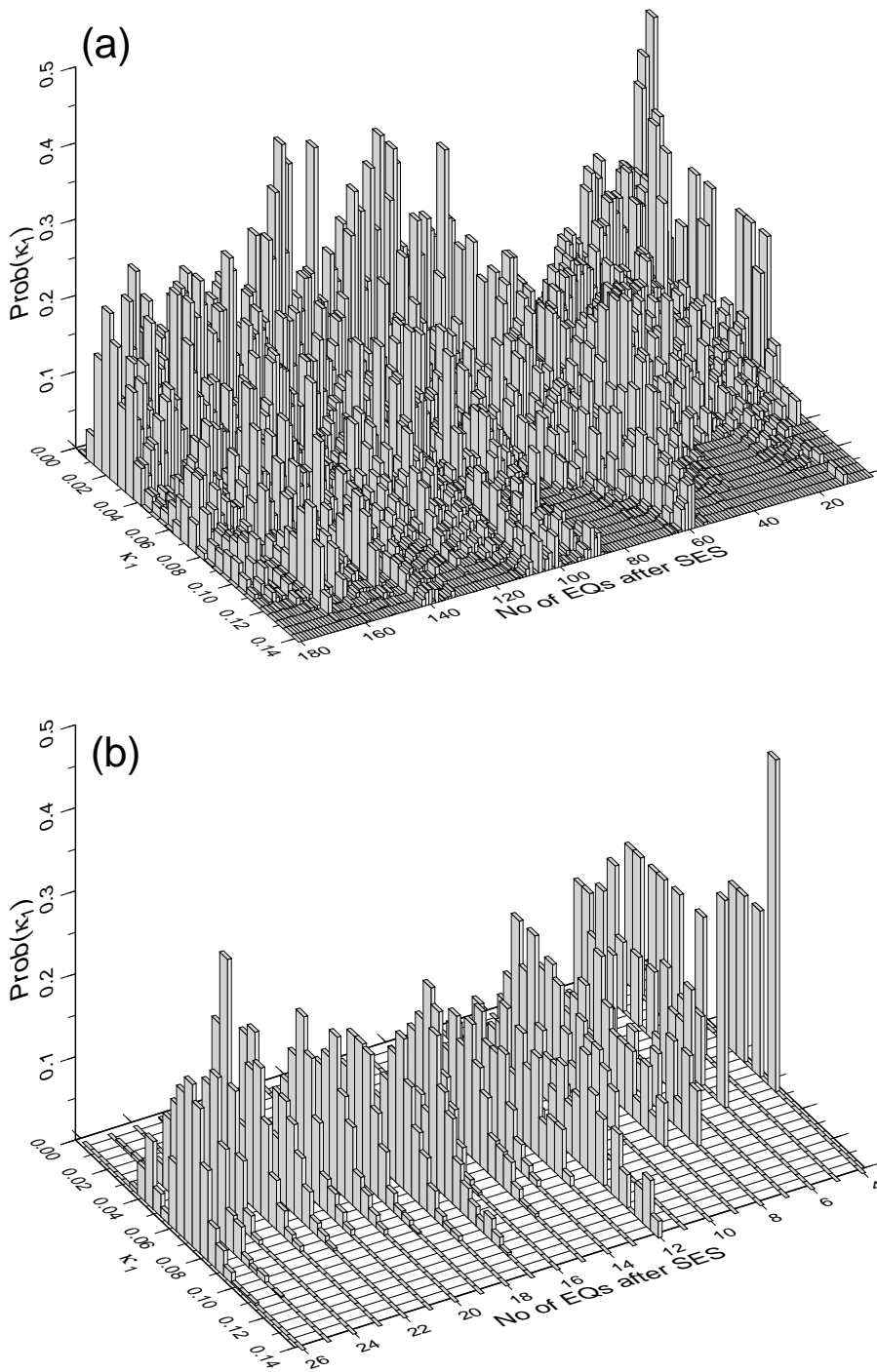


FIG. 11: The same as Fig.9, but for the area $N_{37.65}^{39.00}E_{22.20}^{24.10}$ by considering the seismicity since (a) March 28, 2009 and (b) June 21, 2009 (see the text).

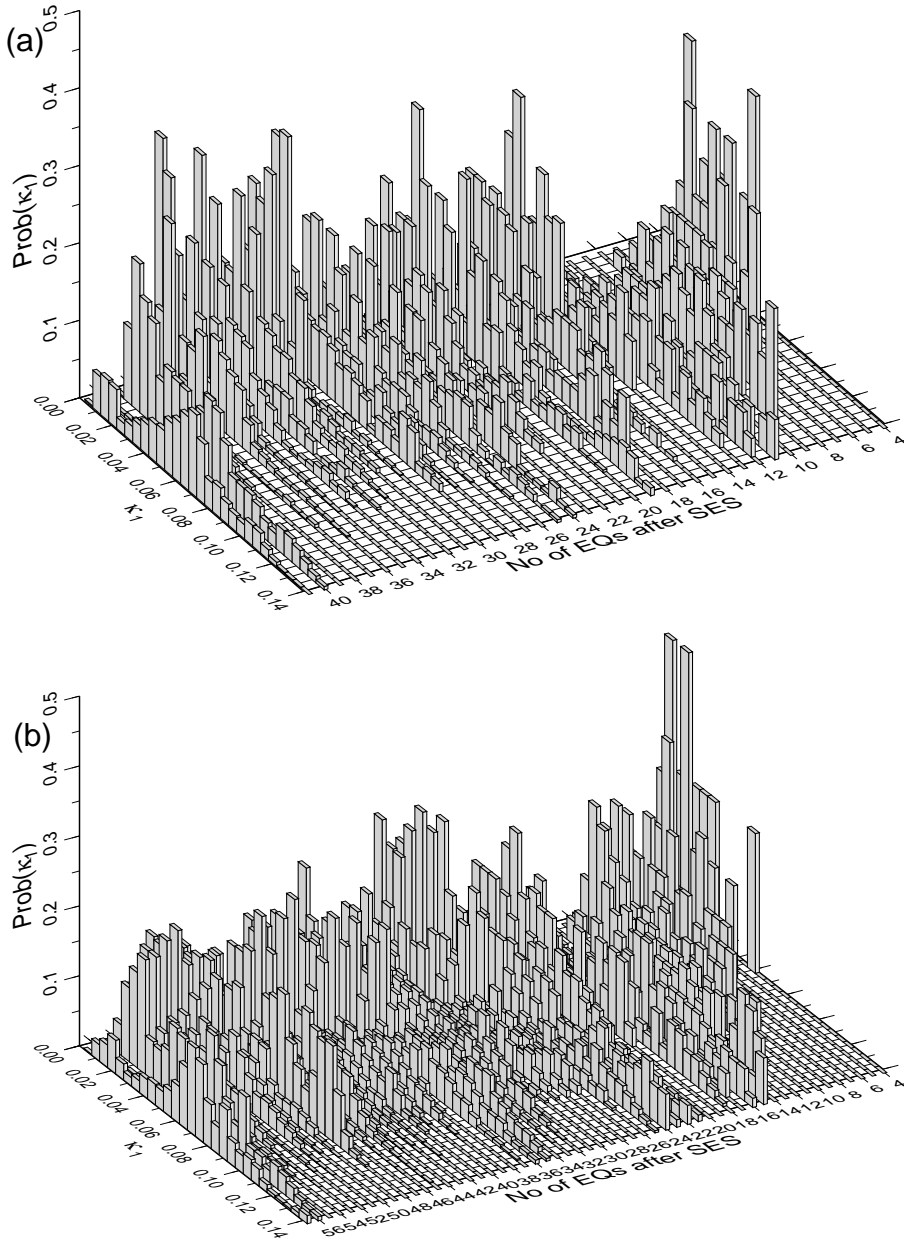


FIG. 12: The probability $\text{Prob}(\kappa_1)$ vs κ_1 upon considering the seismicity ($M_{thres}=3.1$) until 9:35 UT on September 2, 2009: Panel (a) corresponds to the area $N_{37.7}^{38.8}E_{22.6}^{24.1}$, whereas panel (b) to the larger area $N_{37.65}^{39.00}E_{22.20}^{24.10}$.

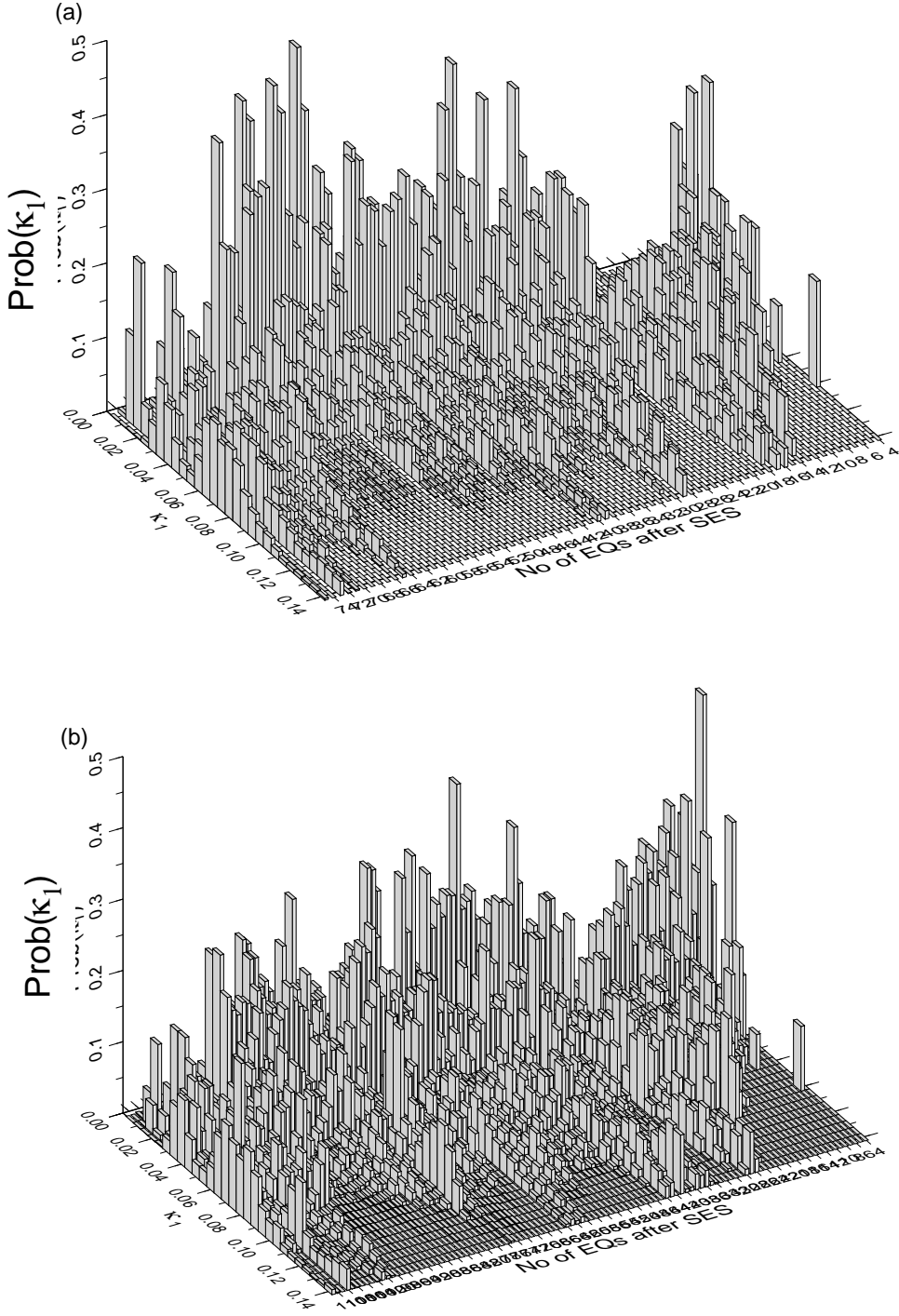


FIG. 13: The probability $\text{Prob}(\kappa_1)$ vs κ_1 upon considering the seismicity ($M_{thres}=3.0$) until 1:55 UT on September 18, 2009: Panel (a) corresponds to the area $N_{37.8}^{38.8}E_{22.6}^{24.1}$, whereas panel (b) to the larger area $N_{37.65}^{39.00}E_{22.20}^{24.10}$.

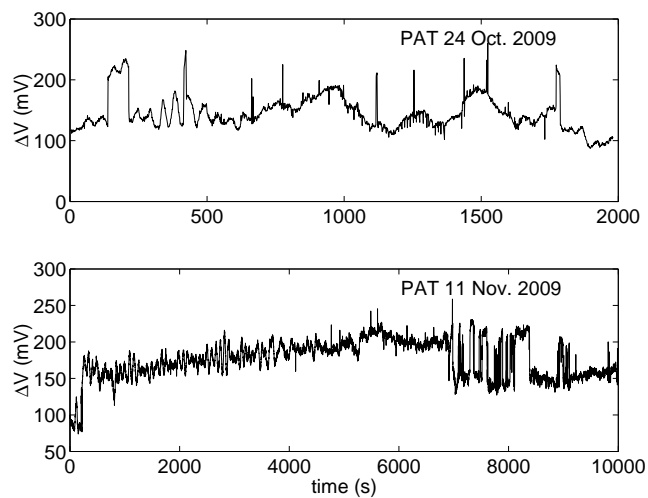


FIG. 14: The SES activities at PAT on 24 October 2009 (upper) and 11 November 2009 (lower), see the text.

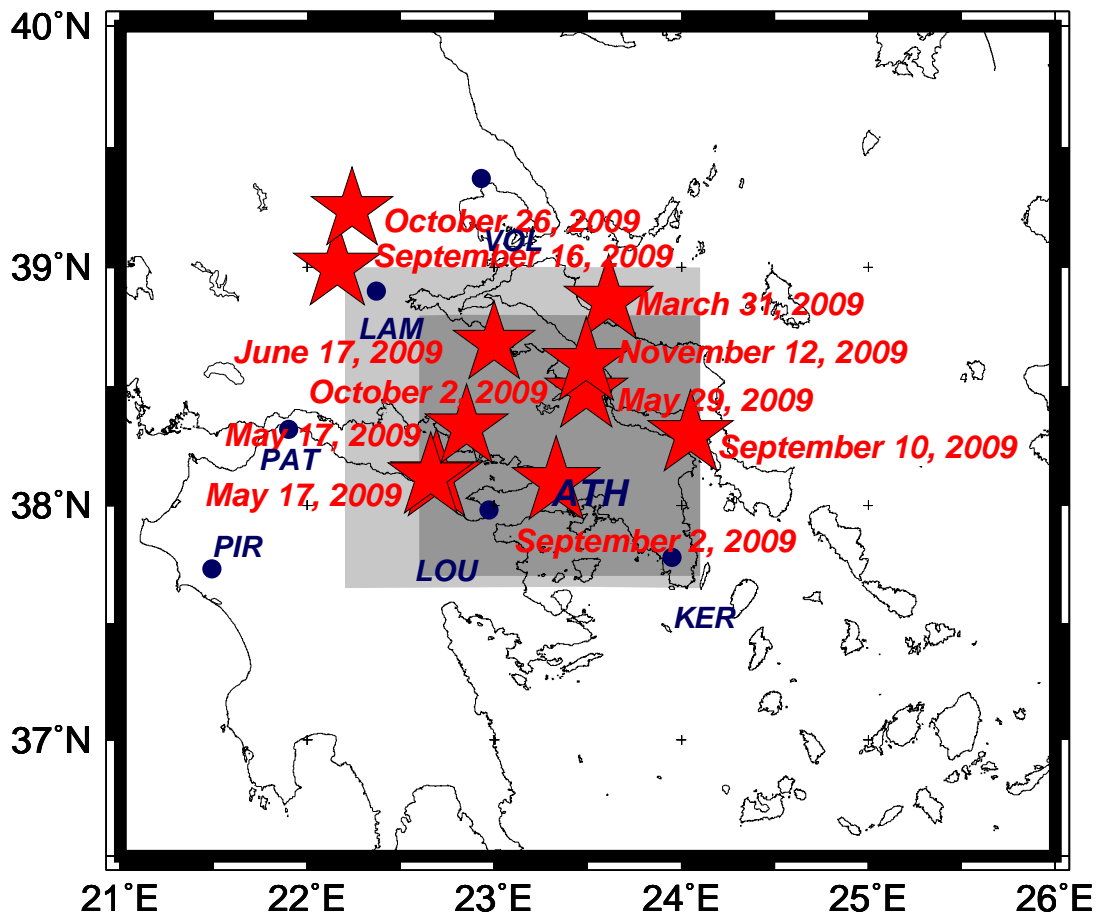


FIG. 15: Earthquakes with magnitude $M_s(\text{ATH}) \geq 4.5$ and epicenters within (or very close to) the area(s) specified in advance that followed the consecutive Notes added to this paper.

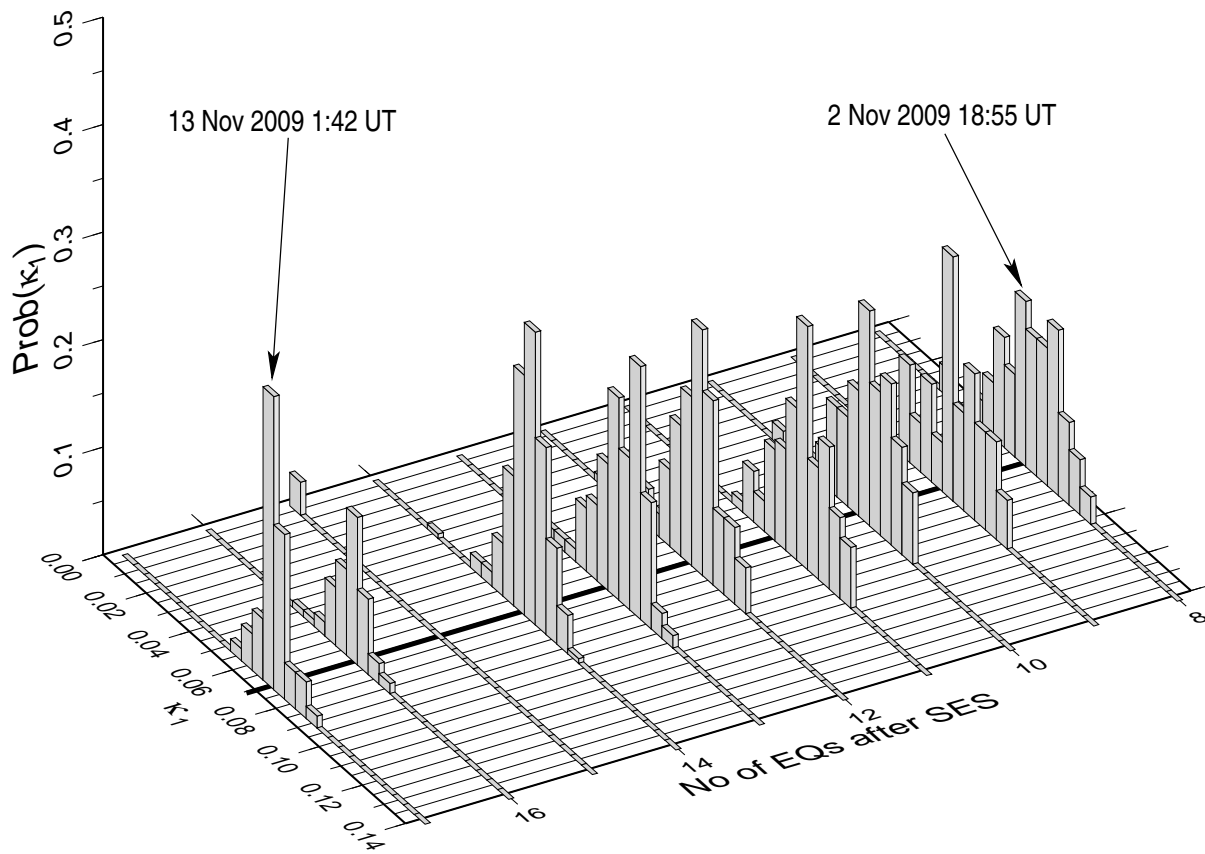


FIG. 16: The probability $\text{Prob}(\kappa_1)$ of the seismicity within the area $N_{37.5}^{38.6}E_{19.8}^{23.3}$ subsequent to the SES activity recorded at PAT on October 24, 2009, when considering $M_{thres}=3.1$. The seismic data until early in the morning on November 13, 2009, have been used.

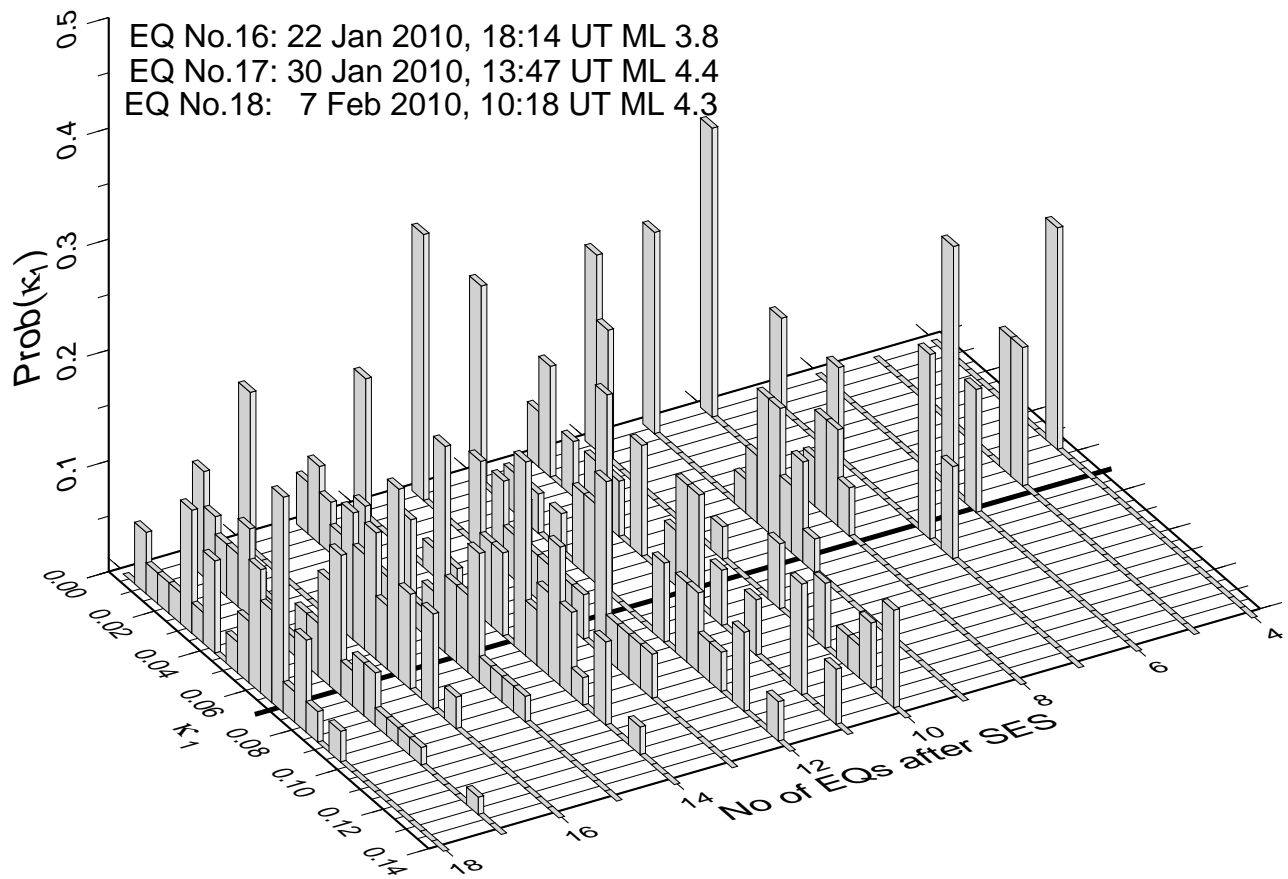


FIG. 17: The probability $\text{Prob}(\kappa_1)$ of the seismicity, for $M_{\text{thres}}=3.5$, within the area $N_{38.0}^{39.0}E_{21.5}^{23.7}$ when considering the seismic data until early in the morning on February 8, 2010.